Chin. J. Astron. Astrophys. Vol. 6 (2006), No. 1, 77–86
(*http://www.chjaa.org*)

Chinese Journal of
Astronomy and
Astrophysics

Energy Buildup, Flux Confinement and Helicity Accumulation in the Solar Corona *

You-Qiu Hu and Wen Li

School of Earth and Space Sciences, University of Science and Technology of China, Hefei 230026; *huyq@ustc.edu.cn*

Received 2005 June 26; accepted 2005 August 16

Abstract Starting from a dipole field and a given distribution of footpoint displacement of field lines on the photosphere, we find axisymmetric, force-free field solutions in spherical coordinates that have the same distribution of normal field on the photosphere and magnetic topology as the dipole field. A photospheric shear is introduced in the azimuthal direction in a region that strides across the equator and ends at latitude λ_s. The footpoint displacement has a sine distribution in latitude and a peak amplitude of φ_m. The magnetic energy E, azimuthal flux F_φ, and magnetic helicity H_T in the solar corona are then calculated for each force-free field solution. It is found that for a given shear region range λ_s, all of the three quantities increase monotonically with increasing φ_m. In particular, both F_φ and H_T have a linear dependence on φ_m. When φ_m reaches a certain critical value φ_{mc}, the force-free field loses equilibrium, leading to a partial opening of the field and the appearance of a current sheet in the equatorial plane. At this point, E, F_φ and H_T reach their maximum values, E_c, $F_{\varphi c}$ and H_{Tc}. E_c increases, and $F_{\varphi c}$ and H_{Tc} decrease with decreasing λ_s. It is found that E_c is always smaller than the open field energy, in agreement with the Aly conjecture. Of the three critical parameters, E_c has the weakest dependence on λ_s. Therefore, if one is interested in the transition of a magnetic configuration from a stable state to a dynamic one, the magnetic energy is probably the most appropriate marker of the transition.

Key words: Sun: magnetic fields — Sun: force-free fields — methods: numerical

1 INTRODUCTION

It is widely believed that solar active phenomena such as coronal mass ejections and solar flares are generated by a sudden release of magnetic free energy stored in the corona (Forbes 2000; Low 2001). Photospheric shear motions may serve as one of the sources that cause the energy buildup in the corona. However, Aly (1984) put forward a conjecture that in an infinite domain and for a given distribution of normal field at the lower boundary, the maximum energy of force-free fields with at least one end of each field line anchored to the lower boundary is the corresponding open field energy. This conjecture was supported by many studies. For instance, Mikić & Linker (1994) investigated the energy buildup of a dipole field through photospheric shear motions, and for a special pattern of shear they found a maximum energy of 0.540 that is slightly (but definitely) below the open field energy 0.554 in units of $4\pi B_0^2 R_\odot^3/\mu$, where B_0 is the field strength at the

∗ Supported by the National Natural Science Foundation of China.

equator, $R_\odot$ is the solar radius, and μ is the vacuum magnetic permeability. Their results are therefore in agreement with the Aly conjecture. Another example was provided by Antiochos et al. (1999), concerning the energy buildup in a field of quadrupolar configuration, where the central arcade is sheared. They argued that the energy of the sheared force-free field is bounded above by the energy of the state in which all the flux in the central and overlying arcades opens, but the flux of the bipolar fields at the flank remains closed. Such an argument was further quantified and then used by Hu (2004) to extend the Aly conjecture from fully open force-free fields to partly open ones in such a way that in the frame of ideal MHD, it is impossible to store more magnetic energy in the corona by photospheric shear motions at the base of any part of the closed flux of a force-free field than that of the field in which the sheared flux opens but the remainder remains closed. Hu & Wang (2005, "Paper I" hereinafter) provided another example in support of Hu's extension.

It is expected the total shear flux confined by a force-free field also has a limit. For axisymmetric force-free fields in spherical coordinates, for instance, the azimuthal flux confined by a fixed poloidal flux must be finite. Flyer et al. (2004) found axisymmetric force-free field solutions, in which the ratio between the two fluxes is around 1.7, being essentially independent of the shear field distribution on the photosphere. These solutions have the same normal field distribution on the photosphere as a dipole field has, but differ in magnetic topology from the dipole field: one or more isolated magnetic islands may appear in the magnetic configuration. If a dipole field is sheared and evolves in the frame of ideal MHD, the magnetic topology of the resulting force-free fields should remain the same as the dipole field. In this situation, it is expected that the maxima of magnetic energy, azimuthal flux and magnetic helicity depend on the pattern of the shear.

This paper starts with a dipole field and introduces a shear displacement along the azimuthal direction in order to study the energy buildup, the confinement of shear flux and the accumulation of magnetic helicity in the corona. It differs from Mikić & Linker (1994) in that the calculations are made for more patterns of footpoint displacements so as to study their effect on the energy buildup, the azimuthal flux confinement and the helicity accumulation. It also differs from Flyer et al. (2004) in the following two aspects. First, the shear is implemented by specifying the footpoint displacement on the photosphere rather than the azimuthal field as a function of the poloidal flux. Secondly, our force-free field solutions preserve the magnetic topology of the dipole field without any isolated islands. The physical model and solution procedures are given in Section 2. We describe the numerical results in Section 3 and conclude our work in Section 4.

2 PHYSICAL MODEL AND SOLUTION PROCEDURES

2.1 Basic Equations for Force-Free Fields

An axisymmetric magnetic field in spherical coordinates (r, θ, φ) may be expressed by

$$\boldsymbol{B} = \nabla \times \left(\frac{\boldsymbol{\psi}}{r \sin\theta} \hat{\varphi} \right) + \boldsymbol{B}_\varphi, \qquad \boldsymbol{B}_\varphi = B_\varphi \hat{\varphi}\,, \tag{1}$$

where ψ is the magnetic flux function and B_φ is the azimuthal component of the magnetic field. The unsheared field is a dipole field, of which $B_\varphi = 0$ and

$$\psi = \frac{\sin^2\theta}{r}\,, \tag{2}$$

where ψ is normalized by a constant flux ψ_0 and r by the solar radius $R_\odot$, so the field strength by $B_0 = \psi_0/R_\odot^2$. The dipole field is then sheared at the coronal base so as to change into a force-free field, whose ψ must satisfy the following partial differential equation:

$$\frac{\partial^2\psi}{\partial r^2} + \frac{\sin\theta}{r^2}\frac{\partial}{\partial\theta}\left(\frac{1}{\sin\theta}\frac{\partial\psi}{\partial\theta}\right) + Q\frac{dQ}{d\psi} = 0\,, \tag{3}$$

where

$$Q = r\sin\theta B_\varphi = Q(\psi) \tag{4}$$

being constant along each field line, and the boundary condition that ψ equals $\sin^2\theta$ at the base. The remaining problem is how to exert a shear of the field.

2.2 Specification of Footpoint Displacement

Mathematically, there are two approaches to shear a field: one, called generating function method in the literature, is to specify the pattern and amplitude of the shear field component, and the other, to specify the footpoint displacement at the coronal base. Flyer et al. (2004) followed the first approach and assumed that

$$Q = \sqrt{\frac{2\gamma}{n+1}}\psi^{(n+1)/2}\,, \tag{5}$$

where γ and n are two free parameters controlling the amplitude and the pattern of the shear. On the other hand, many other authors (e.g., Mikić & Linke 1994; Antiochos et al. 1999; Hu & Wang 2005) chose to specify the footpoint displacement at the base, which seems to be a more appropriate way in modelling solar magnetic fields (Klimchuk & Sturrock 1989). We will take the second approach and follow a special technique proposed by Hu & Wang (2005, "Paper I" hereinafter) to accurately implement numerically a given footpoint displacement distribution at the base.

For all numerical solutions in this study, the footpoint displacement at the base is limited to a region that strides over the equator and ends at latitude λ_s:

$$\delta\varphi(\lambda) = \begin{cases} \varphi_m \sin(\lambda\pi/\lambda_s), & |\lambda| \le \lambda_s, \\ 0, & \text{otherwise,} \end{cases} \tag{6}$$

where $\delta\varphi$ is one half of the footpoint displacement, φ_m is the amplitude, and λ is the latitude ($\lambda = \pi/2 - \theta$). For a sheared force-free field, $\delta\varphi$ is calculated by (Hu 2004; Paper I)

$$\delta\varphi(\psi) = -\int_\psi \frac{B_\varphi d\theta}{\sin\theta B_\theta} = Q(\psi)\int_\psi \frac{d\theta}{\sin\theta\partial\psi/\partial r}\,, \tag{7}$$

where the integration is carried out along the field line from one footpoint to the apex, and Q is defined by Eq. (4). Note that Mikić & Linker (1994) specified the azimuthal velocity at the base, given by

$$v_\varphi^0 = v_0\Theta\exp[(1-\Theta^4)/4], \qquad \Theta = (\theta - 90^\circ)/20^\circ\,,$$

which is equivalent to a specification of the azimuthal displacement of footpoints. Figure 1 shows the two specifications: they are essentially similar in shape. The colatitudinal profile of the footpoint displacement is fixed in Mikić & Linker's calculation, limited to a region $\sim 50^\circ{-}130^\circ$, whereas the range of shear here marked by λ_s is subject to change. In what follows, λ_s is determined by $\psi_s = \sin^2\theta_s$, where $\theta_s = \pi/2 - \lambda_s$, and the values of ψ_s are evenly spaced from 0.1 to 0.8 at intervals of 0.1. Table 1 lists the values of θ_s and λ_s corresponding to the selected values of ψ_s. Obviously, the range of shear increases with decreasing ψ_s or increasing λ_s.

Table 1 Colatitude θ_s and latitude λ_s of the border of the shear region versus $\psi_s = \sin^2\theta_s$

ψ_s	0.1	0.2	0.3	0.4	0.5	0.6	0.7	0.8
$\theta_s(^\circ)$	18.4	26.6	33.2	39.2	45.0	50.8	56.8	63.4
$\lambda_s(^\circ)$	71.6	63.4	56.8	50.8	45.0	39.2	33.2	26.6

2.3 Solution Procedures

Following Paper I, we take a relaxation method based on time-dependent ideal MHD simulations to find axisymmetric force-free field solutions rather than to directly solve the boundary-value problem of Eq. (2) as Flyer et al. (2004) did. We omit to list the 2.5-dimensional ideal MHD equations and refer the reader to Paper I. In order to further reduce the side-effect of the boundary conditions at the top, we take a rather large simulation domain that extends from the coronal base to 80 solar radii, i.e., $1 \le r \le 80$ and $0 \le \theta \le \pi/2$. The domain is discretized into 165×90 grid points. The

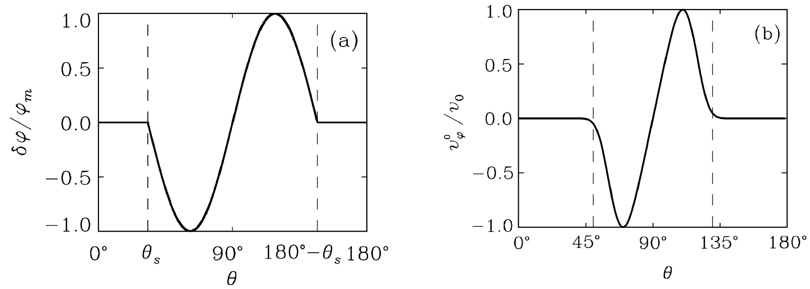

Fig. 1 Colatitudinal profiles of the footpoint displacement given by (a) Eq. (6) and (b) Mikić & Linker (1994). The dashed lines mark the range of the shear region.

grid spacing increases according to a geometrical series of common ratio 1.03 from 0.02 at the base to 0.86 at $r = 30$ and further to 2.28 at the top ($r = 80$), whereas a uniform mesh is adopted in the θ direction. The multistep implicit scheme (Hu 1989) is used to solve the 2.5-D ideal MHD equations. For each set of shear parameters (ψ_s, φ_m), we gradually increase the shear amplitude within 500 characteristic Alfvén transit times to φ_m, so the magnetic configuration undergoes a quasi-static process. Then the simulation continues with φ_m fixed, until the magnetic field reaches a stable state.

A current sheet-like structure may appear along the equatorial plane when the field lines are extremely stretched because of shear with large values of φ_m, and numerical reconnections across it may lead to a change of magnetic topology of the solution. It is easy to figure out a special technique to prevent such reconnections, if one notices that ψ should decrease monotonically with heliocentric distance in the equatorial plane for force-free fields with the same magnetic topology as the dipole field. The approach is then to properly reassign the values of ψ along the equatorial plane to maintain the monotonicity of ψ over there. As a result, the force-free fields obtained are the same as the dipole field in topology.

2.4 Magnetic Energy

When a force-free field solution is obtained, we calculate the magnetic energy E, normalized by $4\pi B_0^2 R_\odot^3/\mu$, according to

$$E = \frac{1}{2}\int_1^{80} dr \int_0^{\pi/2} B^2 r^2 \sin\theta d\theta + \frac{80^3}{2}\int_0^{\pi/2} (B_r^2 - B_\theta^2)_{r=80} \sin\theta d\theta \,, \tag{8}$$

where the first term on the right hand side is the magnetic energy in the simulation domain ($1 \le r \le 80$, $0 \le \theta \le \pi$, $0 \le \varphi \le 2\pi$), and the second is that above the domain, having been transformed into a surface integral over the top (cf. Low & Smith 1993). B_r and B_θ can be evaluated from ψ with the use of Eq. (1), and $B = (B_r^2 + B_\theta^2 + B_\varphi^2)^{1/2}$. B_φ has been ignored in the integrand of the surface integral of Eq. (8) because we are limited to solutions in which the sheared field region lies entirely inside the simulation domain. The contribution of this term is within 10^{-5} for all solutions obtained in this study, so it is our belief that the accuracy of the energy calculation based on Eq. (8) is not affected by the finiteness of the simulation domain and the boundary conditions at the top. For the dipole field and its corresponding open field, the magnetic energy is found to be $E_p = 0.333$ and $E_{\rm Aly} = 0.554$, respectively, with the use of Eq. (8), which agree with those obtained by previous authors (cf. Low & Smith 1993).

2.5 Azimuthal Magnetic Flux

The azimuthal magnetic flux in units of ψ_0 may be evaluated from the force-free field solutions by

$$F_\varphi = \int\int_{r\geq 1} B_\varphi r dr d\theta \, . \tag{9}$$

It is related to $\delta\varphi(\psi)$ by (Hu 2004)

$$F_\varphi = 2\int_{\psi_s}^{1} \delta\varphi(\psi) d\psi \, , \tag{10}$$

where the factor of 2 in front of the integration sign comes from the fact that $\delta\varphi$ is one half of the footpoint displacement (cf. eq. (17) in Hu 2004). Therefore, for $\delta\varphi$ given by Eq. (6) as a function of λ, we may also calculate F_φ, and the result is

$$F_\varphi = k_F(\lambda_s)\varphi_m \, , \tag{11}$$

where

$$k_F(\lambda_s) = \frac{2\pi\lambda_s \sin(2\lambda_s)}{\pi^2 - 4\lambda_s^2} \, . \tag{12}$$

This indicates a linear relation between F_φ and φ_m and the slope depends on the footpoint displacement distribution. For the distribution given by Eq. (6) the slope is a function of λ_s as expressed by Eq. (12). Since we can also use Eq. (9) to calculate F_φ as a function of λ_s from the numerical solutions, the results obtained should be the same as given by Eqs. (11) and (12). This provides a critical criterion in checking the accuracy of these solutions, and the criterion is reasonably fulfilled as will be discussed in next section.

2.6 Magnetic Helicity

Similarly, we may calculate the magnetic helicity of force-free fields in two ways. For two-dimensional force-free fields, Hu et al. (1997) defined a magnetic helicity that is a conserved quantity in the frame of ideal MHD. In spherical coordinates, the newly defined helicity in units of ψ_0^2 is given by

$$H_T = 2\pi \int\int \psi B_\varphi r dr d\theta \, . \tag{13}$$

Inserting Eqs. (9) and (10) into Eq. (13) leads to

$$H_T = 4\pi \int_{\psi_s}^{1} \psi\delta\varphi(\psi) d\psi = k_H(\lambda_s)\varphi_m \, , \tag{14}$$

where $k_H(\lambda_s)$, with the use of Eq. (6), reads

$$k_H(\lambda_s) = \pi^2\lambda_s \left[\frac{2\sin(2\lambda_s)}{\pi^2 - 4\lambda_s^2} + \frac{\sin(4\lambda_s)}{\pi^2 - 16\lambda_s^2}\right] \, . \tag{15}$$

Also, a linear relation exists between H_T and φ_m, and the slope is a function of λ_s given by Eq. (15).

3 NUMERICAL RESULTS

As mentioned above, we have two parameters, ψ_s and φ_m, which control the range and amplitude of the shear at the base. Force-free field solutions are obtained for different combinations of (ψ_s, φ_m). It is found that for each given ψ_s there exists a critical value φ_{mc} such that when φ_m reaches φ_{mc}, the field lines in the outer part of the shear field region are so extremely stretched that a current sheet appears along the equatorial plane and keeps getting longer upward until the stretched field

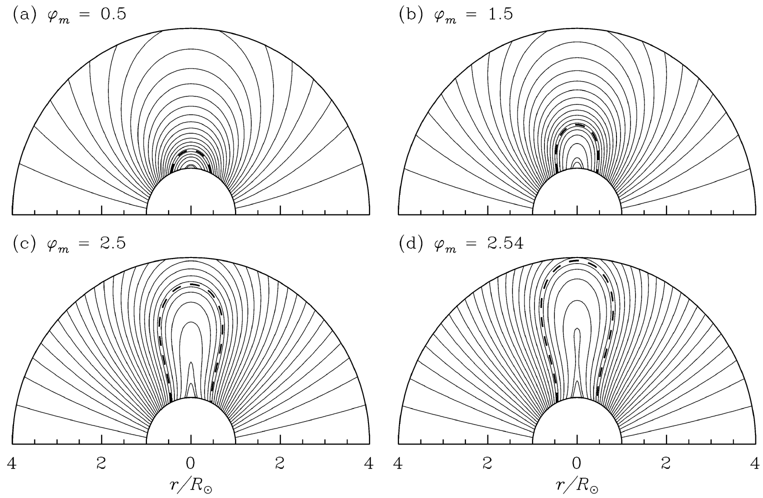

Fig. 2 Magnetic configurations for $\psi_s = 0.8$ and four values of φ_m. Panels (a-c) represent the eventual force-free fields, whereas panel (d) is only an intermediate state. A thick dashed curve in each panel delineates the border of the shear field region.

lines arrive at the top of the simulation domain. To illustrate this process, we show in Figure 2 the magnetic configurations of the series of solutions for $\psi_s = 0.8$ and $\varphi_m = 0.5$, 1.5, 2.5 and 2.54. In the first three cases with $\varphi_m < \varphi_{mc}$, shown in panels (a), (b) and (c), the force-free field reaches a stable state and all field lines remain closed. For the fourth case with $\varphi_m = 2.54$, however, the system loses equilibrium, leading to a partial opening of the field. Figure 2(d) shows only an intermediate state of the field, in which the current sheet is clearly discernible. As the simulation continues, the current sheet keeps extending and the field becomes partly opened. The value of $\varphi_m = 2.54$ is then identified as the critical amplitude φ_{mc}. After the current sheet is fully developed, the magnetic energy, azimuthal flux and magnetic helicity become almost independent of time at values E_c, $F_{\varphi c}$ and H_{Tc}. For this special case, we have $\varphi_{mc} = 2.54$, $E_c = 0.541$, $F_{\varphi c} = 0.64$ and $H_{Tc} = 3.65$.

3.1 Energy Buildup in the Corona

As expected, for a given ψ_s, the magnetic energy E of force-free fields increases monotonically with increasing φ_m. Figure 3(a) shows E as a function of φ_m for $\psi_s = 0.1$, 0.6 and 0.8. Each profile has a termination point at which $E = E_c$. E_c increases monotonically with increasing ψ_s, from 0.514 for $\psi_s = 0.1$ to 0.541 for $\psi_s = 0.8$, as shown in Figure 3(b). The maximum magnetic energy 0.541 in our numerical examples is very close to the value of 0.540 obtained by Mikić & Linker (1994). The range of the shear region at the base shrinks as ψ_s increases, so we conclude that the more the shear is concentrated to the equator, the larger the maximum energy to be stored in the corona will be, a conclusion similar to that obtained by Hu & Wang (Paper I). The dashed line in each panel of Figure 3 denotes the Aly limit ($E_{\rm Aly} = 0.554$), showing that the maximum magnetic energy of these force-free fields are below this limit. This is in agreement with the Aly conjecture.

3.2 Confinement of Azimuthal Magnetic Flux

Flyer et al. (2004) solved Eq. (3) numerically with Q given by Eq. (5), and obtained force-free field solutions with the same distribution of ψ at the base as that of a dipole field. For each sequence of solutions corresponding to a fixed parameter of n, they found that there exists a maximum to the amount of azimuthal magnetic flux confined by a poloidal field of a fixed flux anchored rigidly

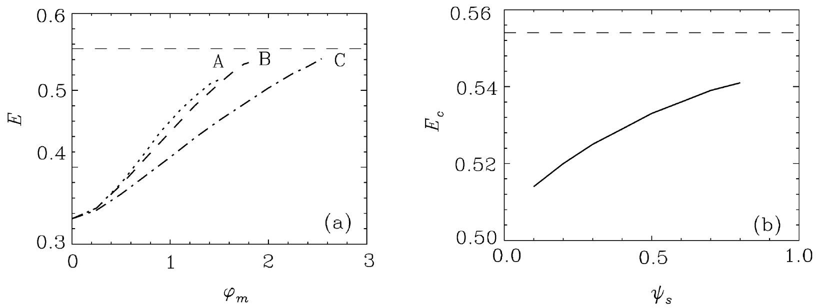

Fig. 3 (a) Magnetic energy E as a function of amplitude φ_m of footpoint displacement for ψ_s = 0.1, 0.6 and 0.8, (b) Maximum energy of the force-free fields versus ψ_s. The dashed line marks the Aly limit ($E_{\rm Aly}$ = 0.554).

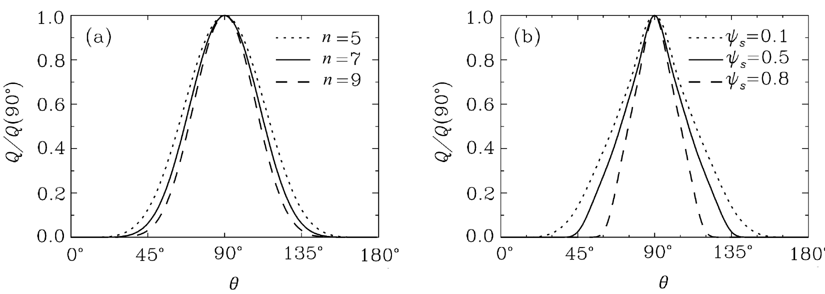

Fig. 4 Colatitudinal profiles of $Q = r \sin\theta B_\varphi$ at tha coronal base for (a) Flyer et al. (2004) and (b) our solutions.

to the coronal base, and that the ratio between the two fluxes is around 1.7, being essentially independent of the value of n in Eq. (5).

As seen from Eq. (5), Q is proportional to $\sin^{n+1}\theta$ at the base, where $\psi = \sin^2\theta$. Figure 4(a) shows the colatitudinal profiles of Q for the cases of n = 5, 7 and 9 discussed by Flyer et al. (2004). For comparison, we calculate Q at the base from our numerical solutions and plot the profiles of Q in Figure 4(b) for ψ_s = 0.1, 0.5 and 0.8. Our profiles are slightly narrower near the equator but similar to theirs as a whole.

Although the distributions of shear field component at the base are similar, our solutions differ from those obtained by Flyer et al. (2004) in the confinement of azimuthal magnetic flux. For each force-free field solution, we calculate F_φ with the use of Eq. (9). Figure 5(a) shows F_φ as a function of φ_m for all values of ψ_s taken in this study. The filled circles represent the numerical values of the examples we have treated, while the straight lines are their optimum least-squares fittings. The linear relation between F_φ and φ_m are well reproduced by our solutions. More quantitatively, we list in Table 2 the slopes of the fitting straight lines and those evaluated from Eq. (12) for different values of ψ_s; the deviations (numerical - analytical) are always negative, and within 0.014 in size. In fact, such deviations can be mostly attributed to the coarseness of the mesh at the base, the spacing being about one degree. The border labelled by λ_s (= $\arccos(\sqrt{\psi_s})$) is not exactly at the grid point, so the numerical border is displaced somewhat inward to a slightly smaller latitude than λ_s. This results in a smaller numerical slope than its analytical counterpart.

Table 2 Slopes of the fitting straight lines in Figures (5) and (6) and evaluated from Eqs. (12) and (15) versus ψ_s.

ψ_s	0.1	0.2	0.3	0.4	0.5	0.6	0.7	0.8
k_F (numerical)	1.290	1.108	0.951	0.797	0.656	0.520	0.386	0.250
k_F (analytical)	1.298	1.120	0.961	0.811	0.667	0.527	0.391	0.259
k_H (numerical)	4.855	4.549	4.223	3.770	3.288	2.747	2.142	1.430
k_H (analytical)	4.861	4.595	4.246	3.822	3.328	2.772	2.162	1.499

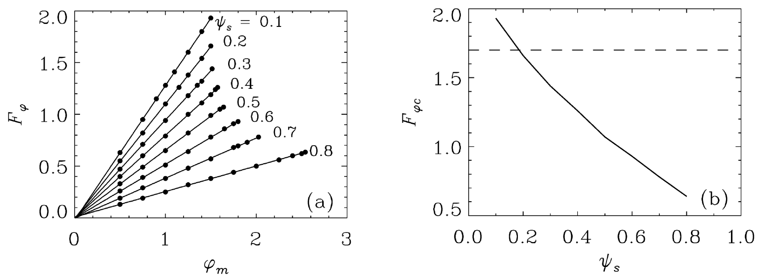

Fig. 5 (a) Azimuthal magnetic flux F_φ as a function of amplitude φ_m of footpoint displacement for different values of ψ_s, (b) Maximum azimuthal magnetic flux $F_{\varphi c}$ versus ψ_s. The filled circles in panel (a) represent the numerical values of the examples treated, and the straight lines are their optimum fittings obtained by the least squares method.

At the termination point of each profile in Figure 5(a), F_φ takes a critical value of $F_{\varphi c}$ as mentioned above. This serves as the maximum azimuthal magnetic flux confined by the poloidal field of unit flux, and it depends on ψ_s. The result is shown in Fig. 5(b), where $F_{\varphi c}$ decreases monotonically with increasing ψ_s, from 1.93 for $\psi_s = 0.1$ to 0.64 for $\psi_s = 0.8$. In other words, the more the shear is concentrated to the equator, the smaller the maximum azimuthal flux confined by the poloidal field will be. This forms a striking contrast to the conclusion reached by Flyer et al. (2004) that the maximum azimuthal flux confined by the poloidal field is around 1.7, and is almost independent of the parameter n which controls the pattern of the distribution of the shear field component at the base (see Eq. (5) and Fig. 4(a)). The reason for this discrepancy is briefly explained below. All force-free field solutions in this study have been obtained by shearing the dipole field at the base and preserving the magnetic topology invariant. No magnetic islands appear in the solutions. However, in the solutions presented by Flyer et al., the magnetic topology is allowed to be different from the dipole field: one or more isolated magnetic islands appear across the equatorial plane (see figs. 4 and 7 of Flyer et al. 2004). A certain amount of azimuthal flux is trapped in these islands, and this plays a compensating role for the reduction of azimuthal flux caused by the concentration of the shear to the equator. For the case that the sheared field is the same as the unsheared in topology, the confined azimuthal flux should depend on the pattern of the distribution of the shear field component at the base, as demonstrated by our solutions.

3.3 Magnetic Helicity Accumulation

It is instructive to examine the maximum magnetic helicity of the force-free fields and its dependence on the shear range parameter ψ_s, since a ceaseless accumulation of helicity in the corona was suggested as a possible mechanism for solar flares and coronal mass ejections (Wang 1992; Low 1994). For each force-free field solution, we calculate H_T with the use of Eq. (13). Figure 6(a) shows H_T as a function of φ_m for all values of ψ_s. Again, the filled circles represent the numerical values of the examples we have treated, while the straight lines are their optimum least-squares fittings. The linear relation between H_T and φ_m is well reproduced by our solutions, too. The numerical slopes, k_H, and their analytical values, given by Eq. (15), are also listed in Table 2. The two sets

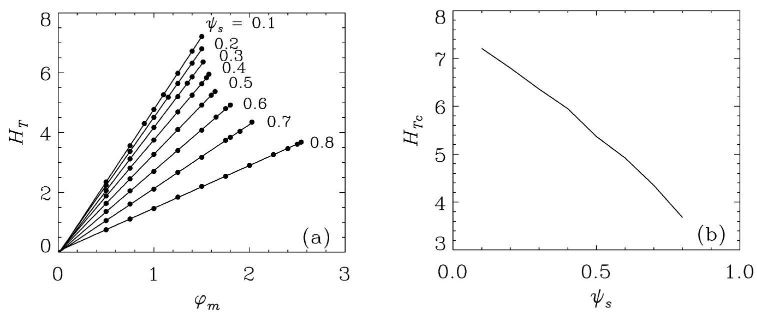

Fig. 6 (a) Magnetic helicity H_T as a function of amplitude φ_m of footpoint displacement for different values of ψ_s, (b) Maximum magnetic helicity H_{Tc} versus ψ_s. The filled circles in panel (a) represent the numerical values of the examples treated, while the straight lines are their optimum least-squares fittings.

of slopes are very close to each other, and the deviations, less than 0.07 in size, stem from the indefiniteness of the border of the shear region, caused by a coarse mesh at the base, as mentioned above.

The value of H_T at the termination point of each profile in Figure 6(a) is the maximum magnetic helicity H_{Tc} of the force-free field, and it depends on ψ_s, as shown in Figure 6(b). H_{Tc} decreases monotonically with increasing ψ_s, from 7.24 for $\psi_s = 0.1$ to 3.65 for $\psi_s = 0.8$. That is, the more the shear is concentrated to the equator, the smaller will be the maximum magnetic helicity of the force-free field.

4 CONCLUDING REMARKS

Using a relaxation method based on 2.5-dimensional, time-dependent ideal MHD simulations in spherical coordinates, we have obtained axisymmetric, force-free field solutions which have the same distribution of normal field component at the coronal base and the same magnetic topology as a dipole field does. Each solution corresponds to a specific sine distribution in latitude of the footpoint displacement at the base, characterized by the latitude λ_s of the border of the shear region and the amplitude φ_m of the displacement. The magnetic energy E, azimuthal flux F_φ, and magnetic helicity H_T are then evaluated from these solutions. The main conclusions are as follows.

(1) For a given λ_s, all of the three quantities increase monotonically with increasing φ_m. In particular, both F_φ and H_T have a linear dependence on φ_m, as proved analytically and demonstrated by the numerical results. The slopes have profiles that depend on the pattern of the footpoint displacement distribution at the coronal base.

(2) For each given λ_s, there exists a critical amplitude φ_{mc} such that when φ_m reaches it, the force-free field loses equilibrium, leading to a partial opening of the field and the appearance of a current sheet in the equatorial plane. At the same time, the magnetic energy, azimuthal flux and magnetic helicity of the force-free field reach their maximum values.

(3) As the shear region shrinks toward the equator, the maximum energy increases, but it is always below the Aly limit. This is in agreement with the Aly conjecture.

(4) The maximum azimuthal flux confined by a poloidal field of unit flux depends on the range of the shear region: it is the less, the more the shear is concentrated to the equator. This differs from Flyer et al.'s (2004) conclusion that the maximum azimuthal flux confinable is almost independent of the shear field distribution. The difference comes from the fact that our solutions have the same magnetic topology as the dipole field, whereas theirs do not.

(5) The maximum magnetic helicity to be accumulated in the corona also depends on the range of the shear region: the more the shear is concentrated to the equator, the less magnetic helicity is allowed to accumulate in the corona.

(6) Of the three critical parameters, the magnetic energy has the weakest dependence on the shear range: it changes from 0.514 to 0.541 when λ_s increases from 0.1 to 0.8. In comparison, the azimuthal flux changes from 1.93 to 0.66, and the magnetic helicity from 7.24 to 3.65. Therefore, if one is specifically interested in the transition of a magnetic configuration from a stable state to a dynamic one, the magnetic energy is probably the most appropriate parameter to mark the transition.

Finally, it should be stressed that both Flyer et al.'s (2004) solutions and ours belong to sub-sets of force-free fields. Flyer et al.'s solutions were obtained in terms of a given pattern of distribution of the shear field component at the base, allowing for a free change of magnetic topology of the field. If one starts from a dipole field, not only a footpoint shear at the base but also a magnetic reconnection somewhere in the corona must be invoked to achieve these solutions. On the other hand, our solutions are implemented through a pure footpoint shear at the base, and consequently, neither magnetic reconnections nor detached flux ropes exist in the corona. The conclusions reached above are then limited to this particular set of force-free field solutions that are formed by a pure shear at the base and do not contain any detached magnetic flux ropes.

Acknowledgements This work was supported by NSFC Grants 40274049 and 10233050, and NKBRSF Grant 2000078404.

References

Aly J. J., 1984, ApJ, 283, 349
Antiochos S. K., DeVore C. R., Klimchuk J. A., 1999, ApJ, 510, 485
Flyer N., Fornberg B., Thomas S., Low B. C., 2004, ApJ, 606, 1210
Forbes T. G., 2000, J. Geophys. Res., 105, 23153
Hu Y. Q., 1989, J. Comp. Phys., 84, 441
Hu Y. Q. 2004, ApJ, 607, 1032
Hu Y. Q., Wang Zh., 2005, ApJ, 623, 551 (Paper I)
Hu Y. Q., Xia L. D., Li X, Wang J. X., Ai G. X., 1997, Solar Phys., 170, 283
Klimchunk J. A., Sturrock P. A., 1989, ApJ, 345, 1034
Low B. C., 1994, In: Proc. of the Third SOHO Workshop - Solar Dynamic Phenomena and Solar Wind Consequences, p.123
Low B. C., 2001, J. Geophys. Res., 106, 25341
Low B. C., Smith D. F., 1993, ApJ, 410, 412
Mikić Z., Linker J. A., 1994, ApJ, 430, 898
Wang J. X., 1992, In: W. R. Hu et al. eds., Advances in Solar Terrestrial Science of China, Beijing: Science Press, p.77